Steel and Composite Structures, *Vol. 36, No. 5 (2020) 587-602*
DOI: https://doi.org/10.12989/scs.2020.36.5.587

Performance of composite frame consisting of steel beams and concrete filled tubes under fire loading

Mahdi Shariati[1], Mohammad Grayeli[2], Ali Shariati*[3,4] and Morteza Naghipour[5]

[1]*Institute of Research and Development, Duy Tan University, Da Nang 550000, Vietnam*
[2]*Mazandaran University of Science and Technology, Babol, Iran*
[3]*Division of Computational Mathematics and Engineering, Institute for Computational Science, Ton Duc Thang University, Ho Chi Minh City 758307, Vietnam*
[4]*Faculty of Civil Engineering, Ton Duc Thang University, Ho Chi Minh City 758307, Vietnam*
[5]*Civil Engineering Faculty, Babol Noshirvani University of Technology, Babol, Iran*

(*Received December 31, 2019, Revised July 26, 2020, Accepted July 29, 2020*)

Abstract. In recent years, the composite columns have been widely used in the structures. These columns are mainly used to construct the structures with a large span and high floor height. Concrete filled tubes (CFTs) are a type of composite column, which are popular nowadays due to their numerous benefits. The purpose of this study is to investigate such frames at elevated temperatures. The method used in this research is based on section 2.2 of Eurocode 4. First, for the verification purpose, a comparison was made between the experimental results and the numerical model of the concrete filled tube. Then a composite frame was analyzed under fire temperature with different parameters. The results showed that the failure time decreased with increasing the friction of different models. Moreover, investigation of the concrete moisture content revealed that an increase in the concrete moisture content from 3% to 10% led to extended failure time for different models. For instance, in the second frame model, the failure time has increased up to 8%.

Keywords: composite sections; concrete filled tube (CFT); frame; fire resistance; FEM modeling; nonlinear analysis

1. Introduction

Concrete filled tubes exhibit an outstanding performance as a member of the building against the accidents and events. Some researchers have worked on the high resistance of CFTs to the earthquake with very good results (Hajjar 2000, Elremaily *et al.* 2002, Han *et al.* 2005, Talebi *et al.* 2018). CFT columns of different circular, square, and rectangular cross-sections have been used in the constructions due to the appropriate performance of concrete and steel against various events and several studies have been carried out on this subject (Han *et al.* 2001, Lam *et al.* 2004, Han *et al.* 2007, Tao *et al.* 2013, Han *et al.* 2014, Lai *et al.* 2014, Abdollahzadeh *et al.* 2018b, Qiao *et al.* 2018, Wang *et al.* 2018). In recent years, concrete filled tubes have become especially popular among designers and engineers. Some special advantages of this type of section include high load-bearing capacity, high seismic resistance, attractive appearance, reduced cross-section, fast construction, and high fire resistance. The concrete in the CFT columns causes a delay in the increased heating of the column section, and the steel tube acts as a shield and prevents the concrete core from being exposed directly to the fire (Twilt *et al.* 1994, Espinos *et al.* 2010). Numerous models of such sections have been developed in the world.

However, some essential features should be incorporated into the models to achieve a more realistic behavior for the performance of these columns against fire. Related aspects such as thermal conductivity and friction model in the concrete and steel interface and thermal expansion coefficient of steel and concrete should be carefully calculated. (Ding *et al.* 2008) developed an advanced 3D model for CFT circular and square columns under fire and examined the thermal gap. (Hong *et al.* 2009) also developed an advanced 3D model to predict the behavior of square CFT columns under fire (Espinos *et al.* 2010). Extensive researches have been carried out on the fire resistance of single-member concrete filled tubes. Lie and Chabot (1990) carried out some experiments on various fillers of steel columns, including plain and reinforced concrete. Also, in the same year, they worked on the methods for predicting the strength of circular concrete-filled tubes (Lie *et al.* 1990a, Lie *et al.* 1990b). Lie and Irwin (1990) evaluated the strength of concrete filled tubes with a rectangular cross-section against fire (Lie *et al.* 1990c). Lie and Denham studied the factors affecting circular RC-filled tubes (Lie *et al.* 1993). Lie and Stringer calculated the strength of the hollow tubes filled with plain concrete under fire (Lie *et al.* 1994). In recent years, Romero et al. worked on elliptical concrete filled tubes (CFTs) and concrete-filled double skin tubes (CFDSTs) under fire (Espinós *et al.* 2014, Romero *et al.* 2015). In another study, Abdollahzadeh and Afaghi studied the effect

*Corresponding author, Ph.D.
E-mail: alishariati@tdtu.edu.vn

ISSN: 1229-9367 (Print), 1598-6233 (Online)

Table 1 Dimensions of models

Column No.	Test Date	Diameter (mm)	Wall Thickness (mm)	Height (mm)	n	N_0 (kN)
C-13	1984-04-10	219.1	4.78	3810	0.27	384
C-17	1984-07-10	219.1	8.18	3810	0.26	525

of dry brick walls on the behavior of concrete-filled tubular columns at elevated temperatures (Abdollahzadeh *et al.* 2018a).

In recent years, artificial intelligence (AI) and classic numerical approaches like optimization methods have been combined together and this leads to making new hybrid techniques that can both optimize and predict the results of various topics in engineering applications. Classic algorithms such as back propagation algorithms have been basically suggested to train artificial neural networks (ANNs) which are the sub-branch of AI. Some disadvantages, such as getting stuck in local extremums and having trouble in crossing plateaus of the error function landscape, are the deficiencies of the classic algorithm. In order to solve these problems, metaheuristic optimization algorithms such as genetic algorithm (GA), particle swarm optimization (PSO), and imperialist competitive algorithm (ICA) can be employed. Applying these techniques could be useful for researchers to predict different characteristics of the CFT columns. The AI method can also be used instead of some dangerous tests such as fire-resistance which could threaten human health (Shariati *et al.* , Shahabi *et al.* 2016, Khorramian *et al.* 2017, Shariat *et al.* 2018, Katebi *et al.* 2019, Mansouri *et al.* 2019, Milovancevic *et al.* 2019, Shariati *et al.* 2019a, Shariati *et al.* 2019b, Shariati *et al.* 2019d, Trung *et al.* 2019, Xu *et al.* 2019, Shariati *et al.* 2020).

Studies have proved that mechanical properties of concrete suddenly drop off at elevated temperatures. However, concrete has an acceptable resistance to fire in comparison to other materials such as wood or steel. The failure of mechanical properties occurs with increasing temperature due to the physicochemical changes in material during the heating process and explosive spalling, which leads to loss of materials, downsizing of sections, and exposure of reinforced steel to extreme temperatures. The spalling risk is affected by various factors, including concrete composition, heating rate, and applied testing approaches. The non-flammable feature (in comparison to wood) and exceptional insulating substance with low thermal diffusivity (compared to steel), are the significant advantages of concrete in the fire. A combination of concrete and steel tubes could improve some mechanical properties, such as compressive strength. CFT also can be used in a more different application than reinforced concrete. In other words, employing CFT can improve the concrete structural performance during and after applying service loads or different kinds of load on concrete. Reinforcing concrete with steel tube is the most applied way to enhance the bending moment and flexibility of concrete as well as to control the crack propagation (Arabnejad Khanouki *et al.* 2010, Arabnejad Khanouki *et al.* 2011, Sinaei *et al.* 2011, Ismail *et al.* 2018, Ziaei-Nia *et al.* 2018, Davoodnabi *et al.* 2019, Luo *et al.* 2019, Sajedi *et al.* 2019, Shariati *et al.* 2019c, Xie *et al.* 2019, Naghipour *et al.* 2020). In this research, Abaqus finite element software was employed for the modeling.

2. CFT column validation

To study the CFT columns under fire loading, two numerical models using Abaqus software were used. The experimental results are compared with the numerical models based on the Lie and Chabot's experiment (Kodur *et al.* 1995). For this verification, two analyses are used: thermal analysis and mechanical analysis.

2.1 Geometry of CFT column model

The verified models are based on a test carried out by (Kodur *et al.* 1995), and their values are given in Table 1. As it is shown in Table 1, N_0 is the axial load applied on the CFT column, n is the axial load intensity equal to N_0/N_u, and N_u is the maximum compressive capacity supported by the column.

2.2. Heat transfer analysis in CFT column

Initially, heat transfer analysis was used to examine node temperature in the models and to find the column temperature at different times. The length of the middle part of the column exposed to fire is 3048 mm. The heat load used in this analysis is uniformly applied to the outer surface of the CFT column, which is based on the ASTM-E119 standard (Talebi *et al.* 2018). The thermal load in accordance with ASTM-E119 (ASTM 2001) can be approximated by the relation (1) taken from the experiment (Kodur *et al.* 1995),

$$T_f = 20 + 750\left[1 - exp\left(-3.79533\sqrt{t}\right)\right] + 170.41\sqrt{t} \quad (1)$$

Where T_f is the fire temperature and t is time.

The 8-node solid mesh (DC3D8) is used for the concrete core and steel tube. The results of the study are applied to the model as the thermal load in the mechanical analysis.

2.3 Mechanical analysis

In this study, the 8-node solid mesh (DC3D8) is implemented for concrete and steel materials. Also for the loading plate, use has been made of the 8-node reduced integration solid mesh (Fig. 1). The maximum size of mesh

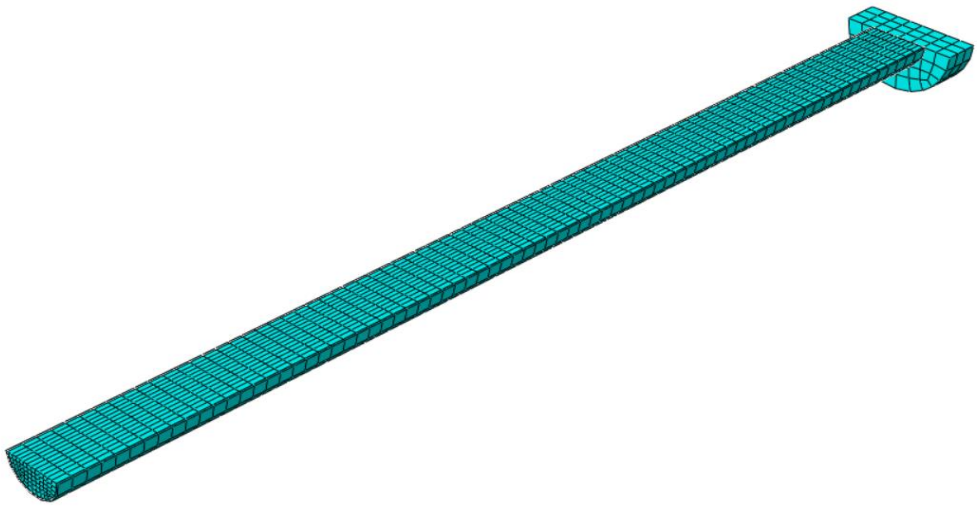

Fig. 1 Meshing model of column C-17

density considered for the prediction of the thermal and mechanical behavior of the numerical model of CFT is 20 cm, which provides good results. One step was used to apply both axial load and the results of heat analysis. To apply the results of the thermal analysis, a predefined field was employed.

2.4 Specifications of concrete and steel at high temperatures

The studied numerical models are dependent on mechanical and thermal properties. The thermal and mechanical properties of steel are derived from EN 1993-1-2 (En 2005). The mechanical properties of concrete are taken from Lie (Lie 1994), as expressed in Eq. (2), and the thermal properties are derived from EN 1992-1-2 (Standardization 2004).

$$\varepsilon_c \le \varepsilon_{max}$$

$$f_c = f_c'[1 - (\frac{\varepsilon_{max} - \varepsilon_c}{\varepsilon_{max}})^2]$$

$$\varepsilon_c > \varepsilon_{max}$$

$$f_c = f_c'[1 - (\frac{\varepsilon_c - \varepsilon_{max}}{3\varepsilon_{max}})^2]$$

and (2)

$$\varepsilon_{max} = 0.0025 + (0.6T + 0.04T^2) \times 10^{-6}$$

$$f_c' = f_{co}' \quad , \quad 0 < T < 450$$

$$f_c' = f_{co}'\left[2.011 - 2.353\left(\frac{T-20}{1000}\right)\right] \quad , \quad 450 \le T \le 874$$

$$f_c' = 0 \quad , \quad T > 874$$

Where f_c and ε_c are the stresses and strains, f_c' is the cylinder strength of concrete at high temperature, f_{co}' is the cylinder strength of concrete at ambient temperature, and T is the temperature in °C.

The thermal expansion coefficient of concrete, according to the suggestion by (Hong *et al.* 2009) was $\alpha_c = 6 \times 10^{-6}$. The moisture content of concrete is applied through specific heat in thermal analysis, which was assumed as 3% in the validation results. The concrete modulus of elasticity is derived from EN 1992-1-1 (EN 2004). The Poisson ratio for concrete is 0.2, and the concrete stress and strain relations are derived from Lie.

2.5 Thermal and mechanical interaction in CFT column between steel tube and concrete

The considered amount of radiation-conduction parameter for the steel tube exposed to fire is 0.5. Also, the amount of heat transfer from the steel tube to concrete was regarded as a coefficient of 25 w/m^{2}k. The thermal resistance between concrete and steel is equal to the constant value of h_j = 200 w/m^{2}k. Two types of reactions are considered between concrete and steel tube, which are as follows: the "hard contact" rule that is considered for normal behavior and the friction coefficient of 0.3 was supposed for the tangential behavior. There is a weld joint between the loading plate and the column steel tube.

2.6 Primary geometric defect in CFT column

Due to the flaws in the manufacturing process, the columns have some defects. In order to consider these drawbacks, a buckling analysis is performed for the column. In order to account for the initial imperfection, the first mode shape of the column is applied using the coefficient of L/1000 as the initial condition for the mechanical analysis, where L is the column length. The first mode shape of the column is obtained from buckling analysis (Talebi *et al.* 2018). In this study, the L/1000 coefficient was used.

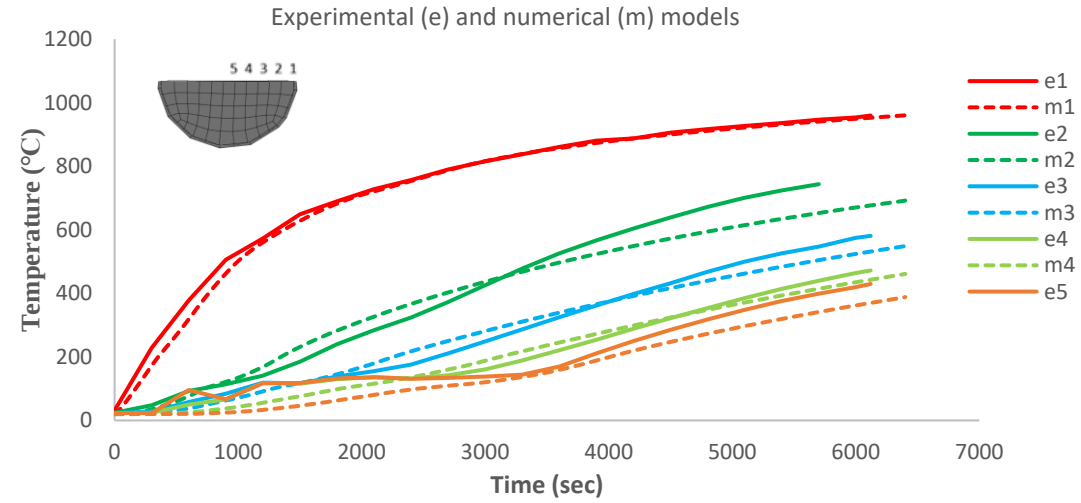

(a)

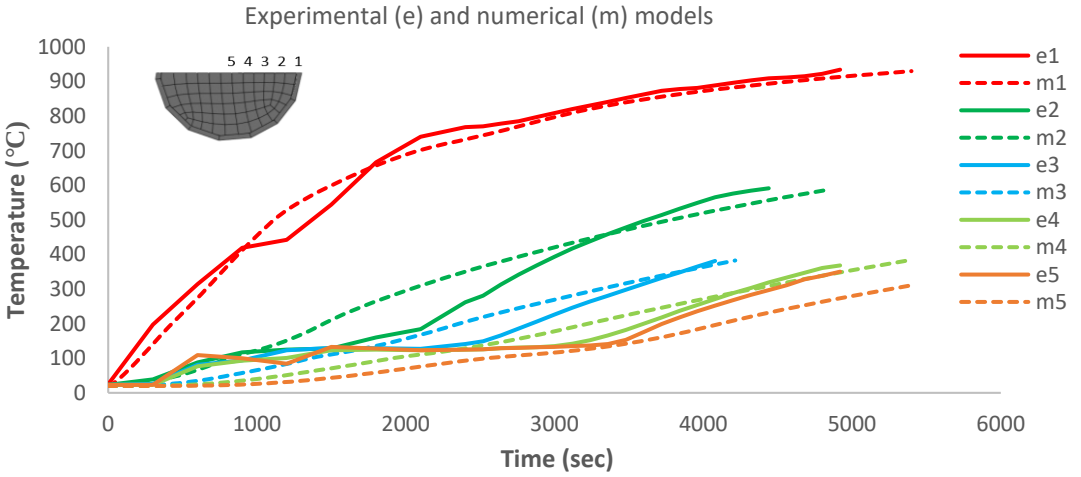

(b)

Fig. 2 Comparison of the temperature-time chart for numerical and experimental models: (a) C-13 and (b) C-17

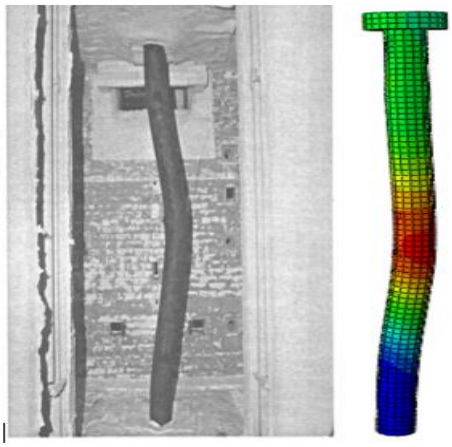

(a) (b)

Fig. 3 Column No C-17 after fire test: (a) experimental model (Kodur *et al.* 1995) (b) numerical model

2.7 Validation

The comparison of numerical and experimental results indicates the consistency and accuracy of the obtained results. Two types of validation have been considered; one based on the heat transfer analysis, and the other derived from the mechanical analysis. In the experiment conducted

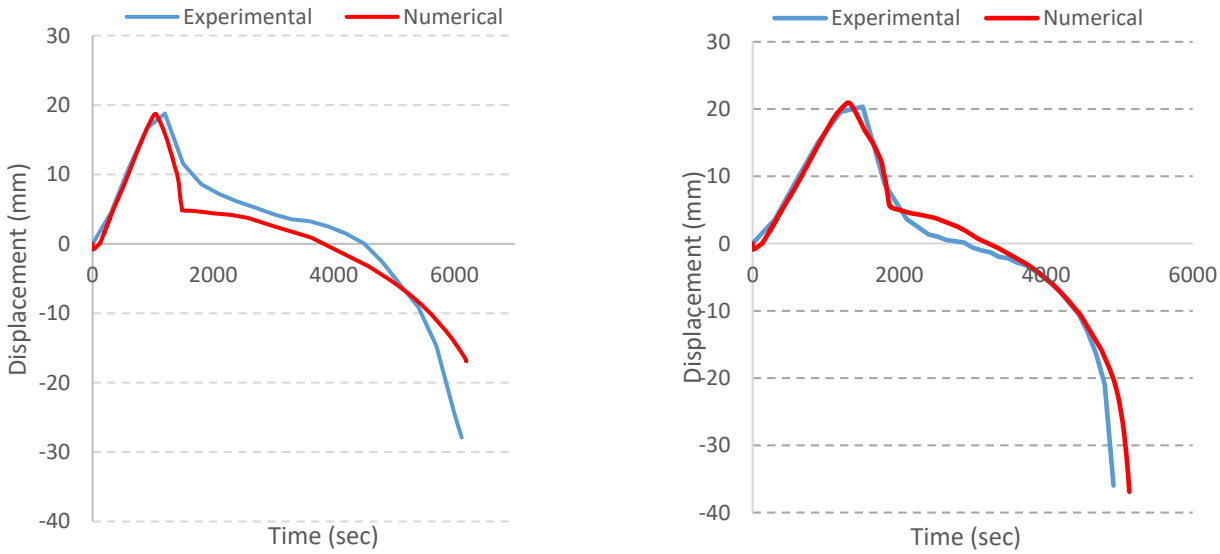

Fig. 4 Comparison of the displacement-time chart for numerical and experimental models: (a) C-13 and (b) C-17

by Lie, thermocouples were embedded in the cross-section of the column to obtain the temperature. The temperature of 5 points was compared between the numerical and experimental models, which can be seen in Fig. (2). Fig. (3) shows the CFT column images after the fire test in the experimental and numerical models. Fig. (4) shows the chart of mechanical analysis, which is a comparison between the displacement of experimental and numerical models over time.

3. The numerical model of the frame under fire loading

In this research, a composite frame consisting of a steel beam connected to a CFT column is completely exposed to fire in order that the beam and the steel tube are under the direct heat of the fire. Besides, the models were subjected to fire loading for 4000 seconds.

3.1 Steel beam-column connection

The steel beam is composed of three parts that are welded to each other (Han *et al.* 2008), which are rectangular steel-made plates. The connection of the steel beam to the concrete-filled steel column was performed through welding, which was modeled using the TIE constrain in ABAQUS (Han *et al.* 2008).

3.2 Numerical model details for the frame

The geometry of the frames and the compressive strength of the beam and steel tube are derived from Han's paper (Han *et al.* 2008). In Table 2, N_0 is the axial load applied on the frame CFT column, n is the axial load intensity equal to N_0/N_u, and N_u is the maximum compressive capacity supported by the column.

Table 2 Axial load of frames

Frame	N_0 (kn)	n
Frame1	285	0.3
Frame2	570	0.6
Frame3	750	0.6

Table 3 Specifications of steel column and beam

	Frame	$f_{ys(mpa)}$	$t_{(mm)}$	υ_s
Beam	1,2,3	303	3.44	0.262
	Frame	$f_{ys(mpa)}$	$t_{(mm)}$	υ_s
Column	3	361	3.46	0.261
	1,2	404	3.46	0.278

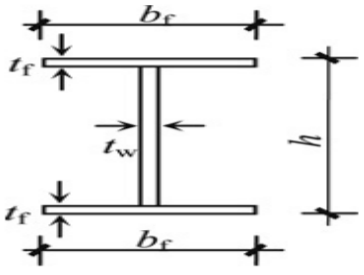

Fig. 5 Schematic image of the composite frame beam (Han *et al.* 2008)

Table 3 shows the yield stress of steel column and beam as well as the Poisson ratio. Fig. (5) is the schematic image of a frame beam. Table 4 shows the dimensions of the column and beam. Also, Fig. (6) shows the numerical model image

Table 4 Various dimensions of frame

Frame1	Column	$B_{(mm)}$	$t_{(mm)}$	$L_{(mm)}$		
		120	3.46	1450		
	Beam	$h_{(mm)}$	$b_{f(mm)}$	$t_{w(mm)}$	$t_{f(mm)}$	$L_{(mm)}$
		160	80	3.44	3.44	2500
Frame2	Column	$B_{(mm)}$	$t_{(mm)}$	$L_{(mm)}$		
		120	3.46	1450		
	Beam	$h_{(mm)}$	$b_{f(mm)}$	$t_{w(mm)}$	$t_{f(mm)}$	$L_{(mm)}$
		140	70	3.44	3.44	2500
Frame3	Column	$B_{(mm)}$	$t_{(mm)}$	$L_{(mm)}$		
		140	4	1450		
	Beam	$h_{(mm)}$	$b_{f(mm)}$	$t_{w(mm)}$	$t_{f(mm)}$	$L_{(mm)}$
		160	80	3.44	3.44	2500

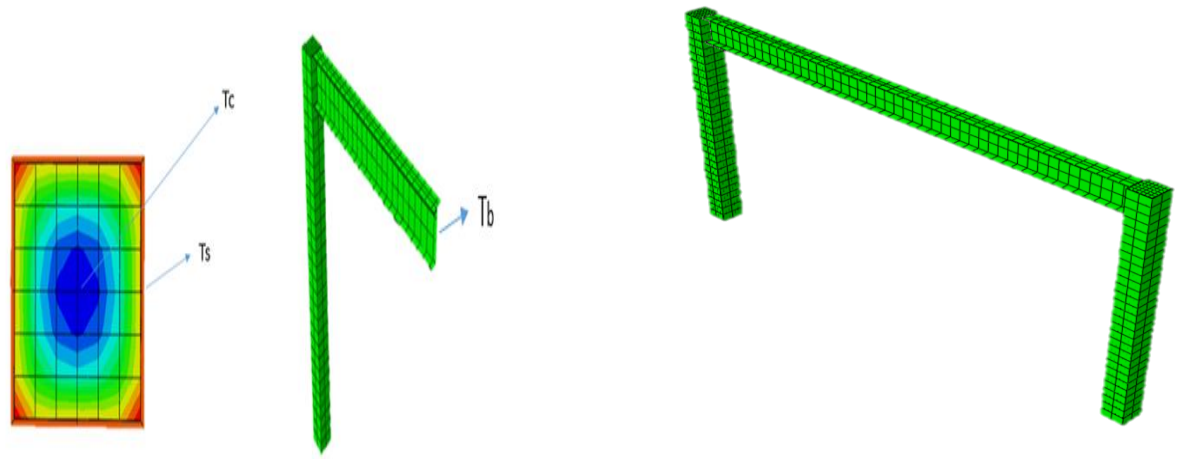

(a) (b)

Fig. 6 (a) Frame image in the numerical model; (b) Specified points for obtaining node temperature; T_c: concrete temperature, T_s: Steel column temperature, T_b: beam temperature

of the frame as well as 3 points of the frame where the temperature is checked. These points include the midpoint in the cross-section of the column for concrete and steel and the midpoint in the middle of the beam.

3.3 Performance of frame with different compressive strength of concrete

In order to show the mechanical behavior of composite frames under fire loading, the axial force-displacement chart is used. The compressive strength of m1 and m2 models are 31.7 and 27.2 MPa, respectively. The Poisson ratio is considered 0.2 for concrete. Fig. 7 shows the frames with different compressive strength of concrete.

3.4 Effect of concrete moisture content on frames

The moisture content of concrete is applied to the thermal analysis through the specific heat. The maximum effect of the concrete moisture content is 100-200°C, with the peak point occurring at 115°C (EN 1994). In the temperature range of 100-200°C, the evaporation occurs in the layers of concrete, resulting in the greatest effect of moisture between these two temperatures. According to the section 2.1 of Eurocode 4, the considered peak for concrete with 3% moisture content is 2020 J/kg.k, and for concrete with 10% moisture content, according to Eurocode 4, the peak is 5600 J/kg.k, as shown in Fig. 8. In the models, m1 is a concrete with a moisture content of 3%, and m2 is a concrete with a moisture content of 10%. Fig. 9 shows a view of the numerical model for the composite frame in the thermal analysis. Fig. 10 shows the results of frame analysis according to the different moisture contents of concrete. The points used for the node temperature are shown in Fig. 6.

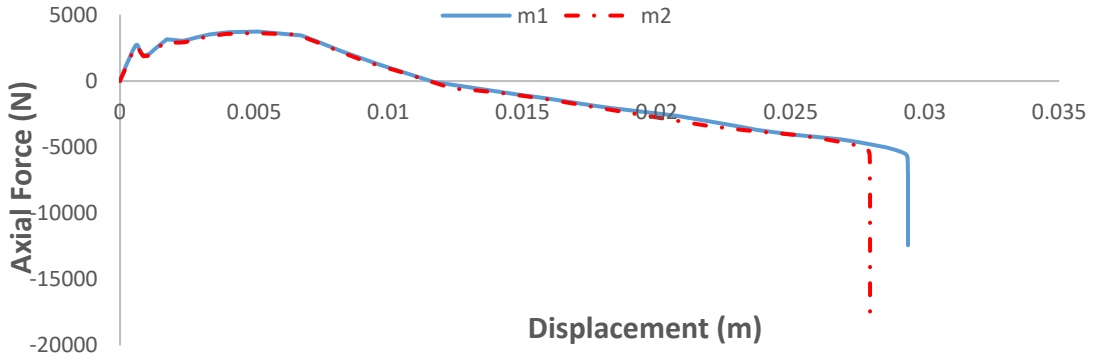

(a) Frame1

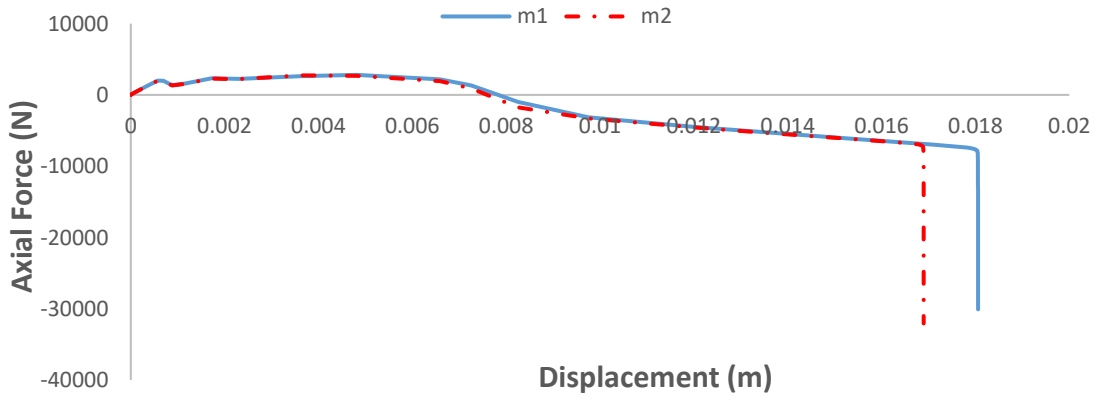

(b) Frame2

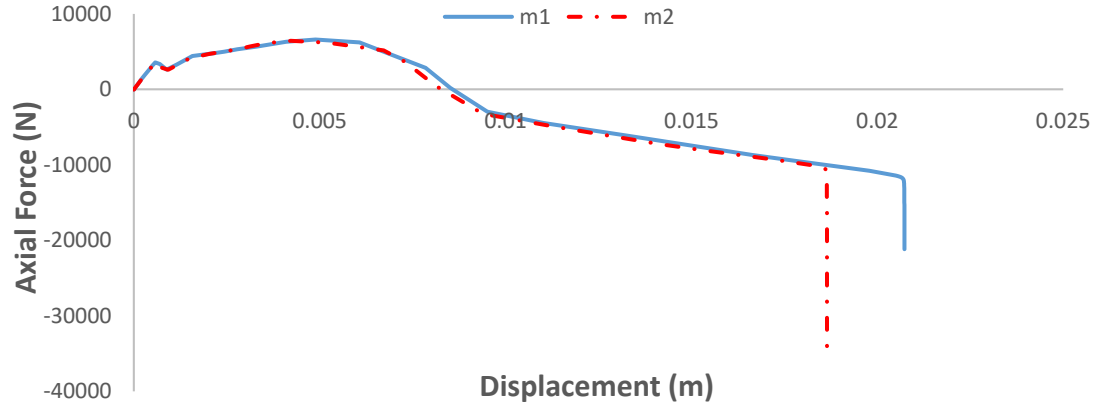

(c) Frame3

Fig. 7 Axial force-displacement chart of frames with different compressive strengths of concrete: (a) Frame1, (b) Frame2 and (c) Frame 3

3.5 Thermal conductivity in frames

In this paper, the thermal conductivity of (Lie 1994) was compared with Eurocode for numerical models. The thermal conductivities mentioned in the Eurocode and Lie was considered based on Fig. 11. The obtained results of this study are shown in Fig. 12. The points used for the node temperature are depicted in Fig. 6.

3.6 Effect of friction coefficient on frames

Two cases are investigated for the friction effect between concrete and steel. The first case is related to the Coulomb friction, and the second one is the full slip between concrete and steel. Coulomb coefficients used in the numerical models are 0.25, 0.5, and 0.75. The full slip shows that there is no friction between concrete and steel. Fig. 13 shows a view of the numerical model for the first frame. Fig. 14 shows the results of the study for the effect of friction coefficients on the frames.

3.7. Effect of thermal expansion coefficient on frames

Two types of thermal expansion coefficients were

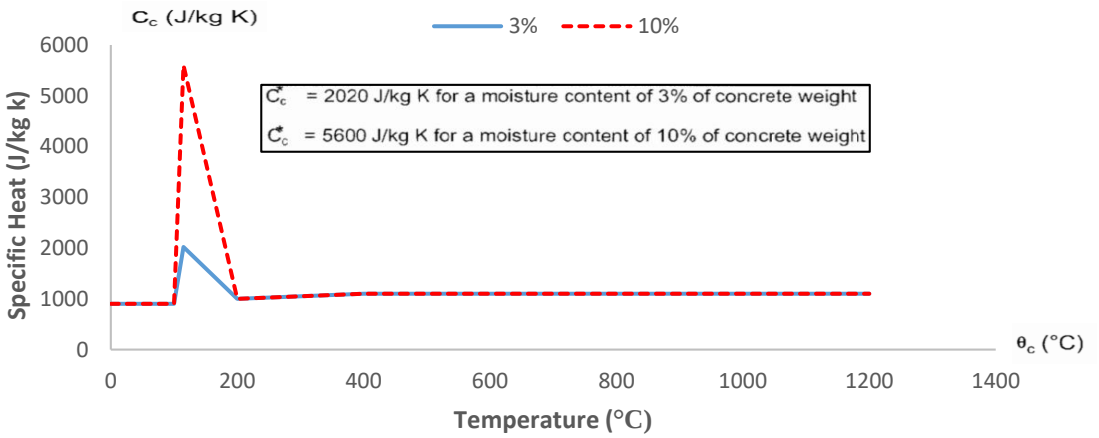

Fig. 8 Special heat-temperature chart for concrete with 3 and 10% moisture (EN 1994)

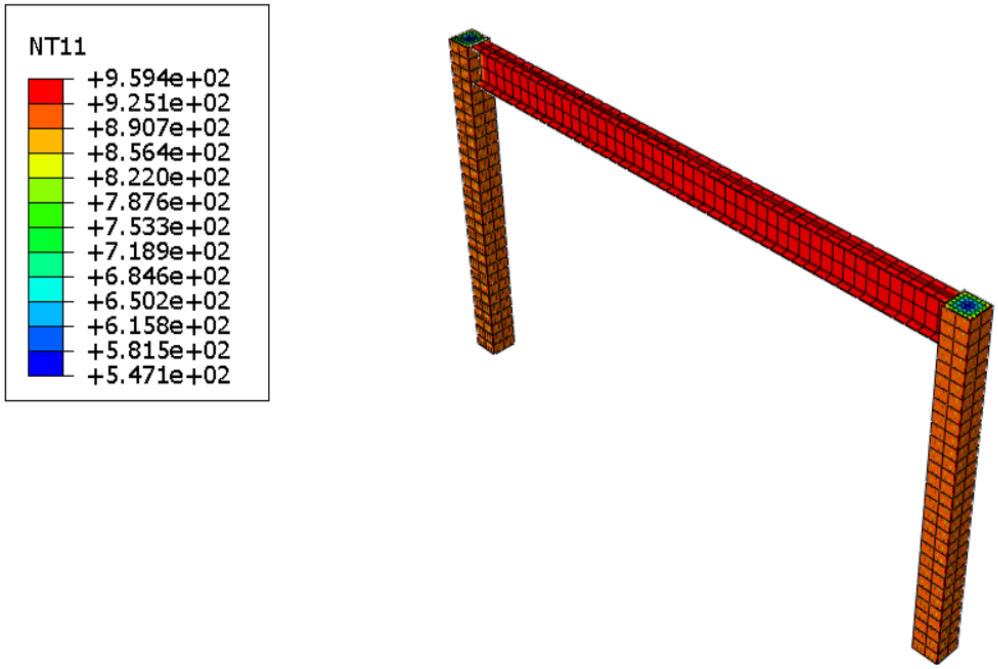

Fig. 9 View of the numerical model for the composite frame in thermal analysis

investigated for concrete and steel in the numerical models, which include constant and variable-temperature. The constant thermal expansion coefficient for concrete is $\alpha_c = 6 \times 10^{-6}$ °C^{-1} and for steel is $\alpha_s = 12 \times 10^{-6}$ °C^{-1}. These values were suggested by (Espinos *et al.* 2010). The variable-temperature thermal expansion coefficient for concrete and steel is taken from Lie [53]. Fig. 15 shows the results of numerical model for the frames.

3.8 The thermal gap in frames

The existing mathematical models for predicting the temperature field in the concrete filled tubes cannot explain the resistance of the heat flow in the concrete-steel interface, which leads to a significant difference between the measured and the predicted temperature. This heat flow resistance is known as the thermal contact resistance. The amount of thermal gap suggested by (Ding *et al.* 2008) is 200 w/m^{2}k (Espinos *et al.* 2010). The thermal gap values of 100, 200, and 500 w/m^{2}k were investigated for the models. The points used for node temperature are described in Fig. 6. Fig. 16 shows the results of the effect of different thermal gaps on heat transfer and mechanical analyses.

Table 5 shows the resistance time of models to fire, which is derived from the axial force-displacement charts of the studied parameters. The models are heated up to 4000 seconds.

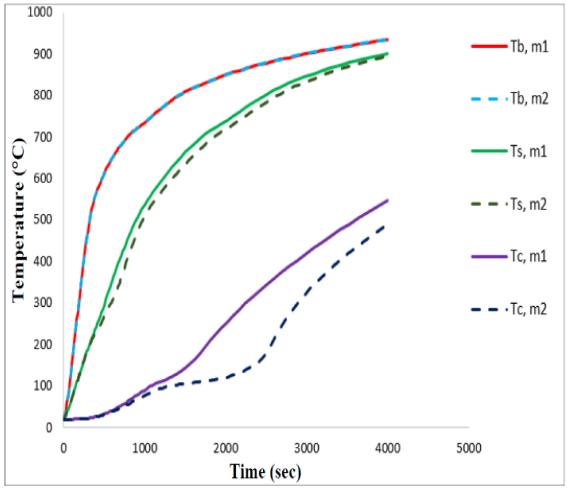

(a) Frame1

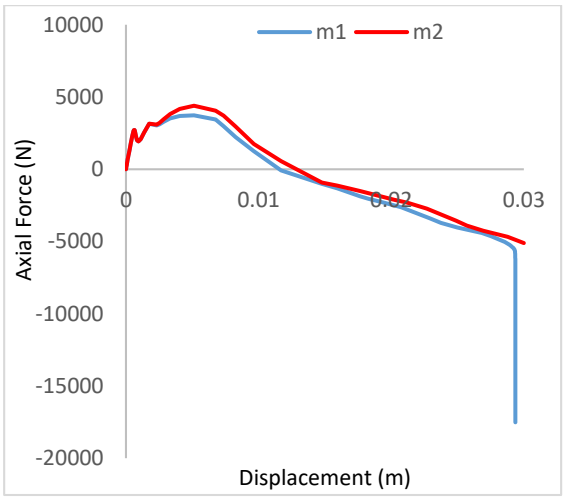

(b) Frame1

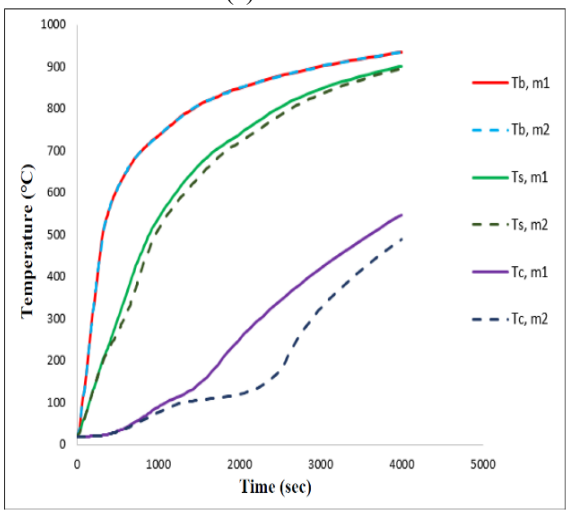

(c) Frame2

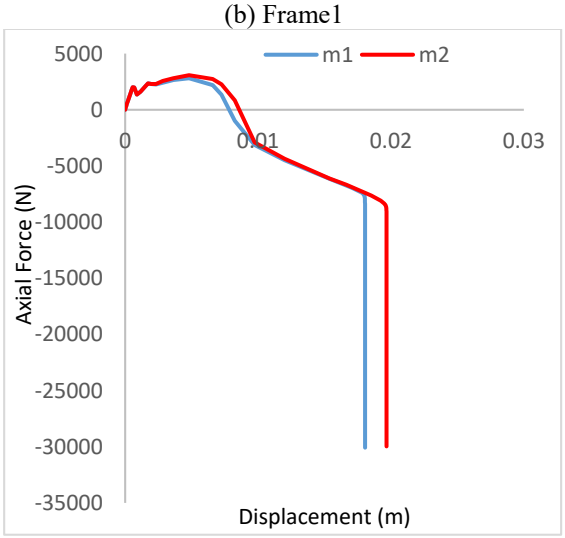

(d) Frame2

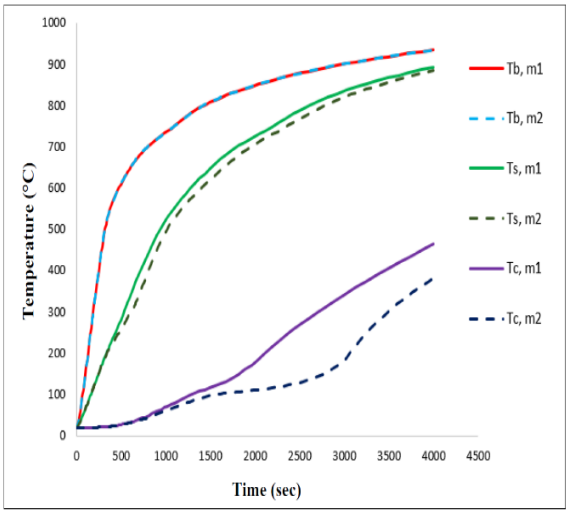

(e) Frame3

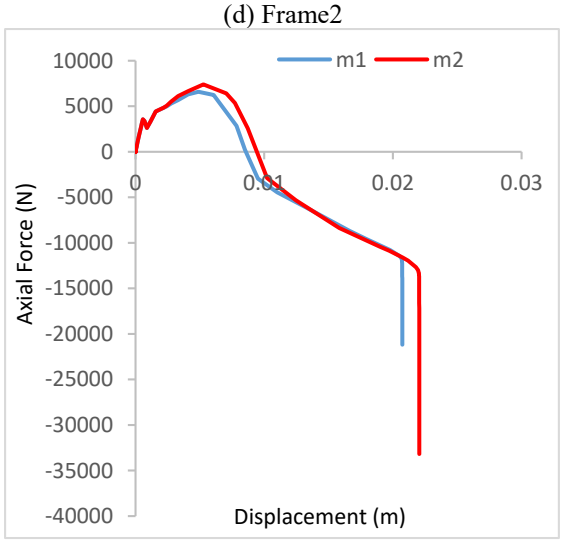

(f) Frame3

Fig. 10 Comparison of node temperature of points determined in m1 and m2 models in frames (a), (c), (e), and comparison of axial force-displacement of m1 and m2 models in frames (b), (d), (f)

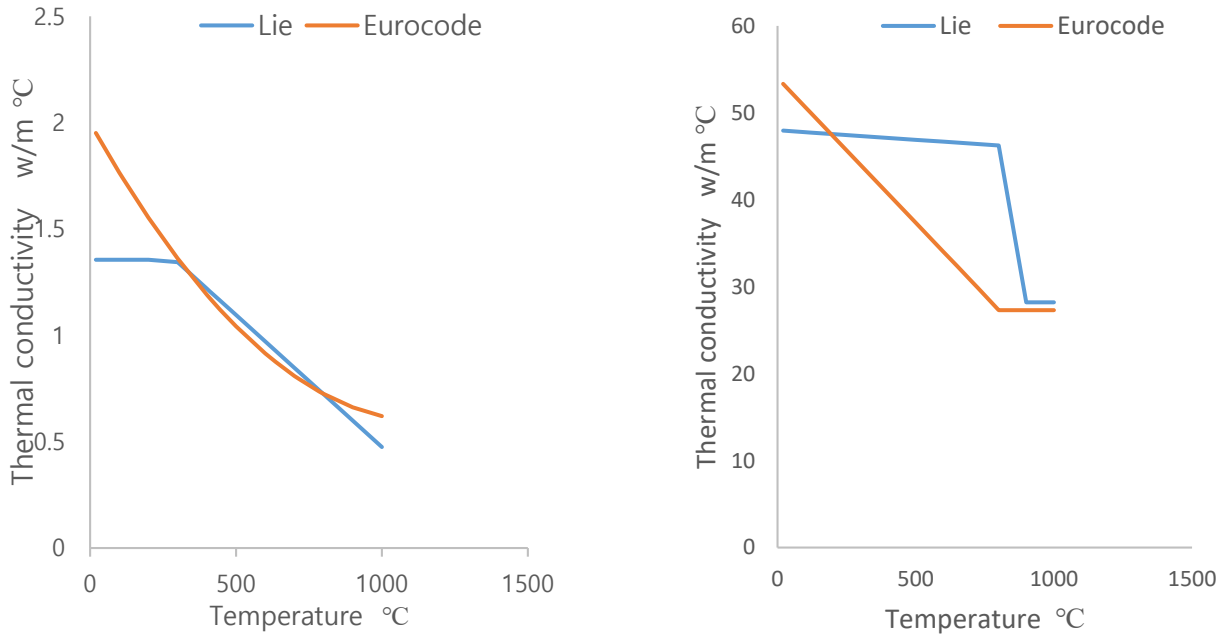

(a) (b)

Fig. 11 Thermal conductivity: (a) concrete (b) steel

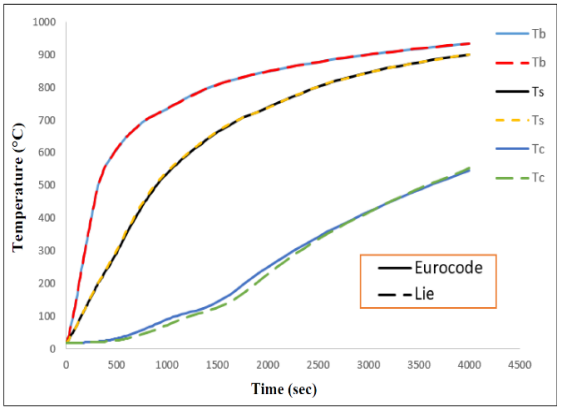

(a) Frame1

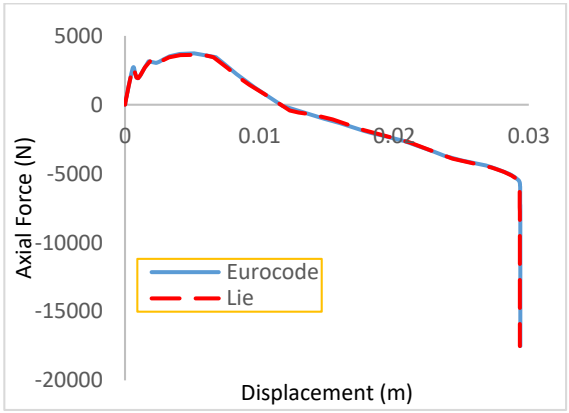

(b) Frame1

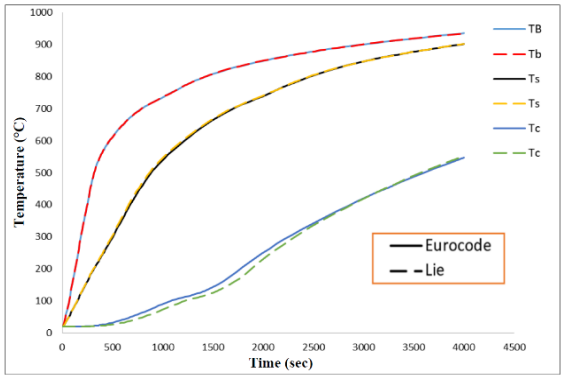

(c) Frame2

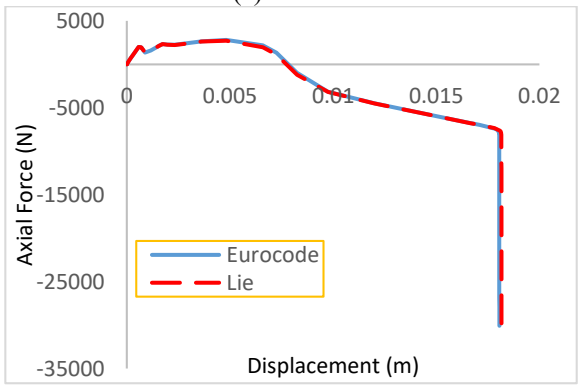

(d) Frame2

Continued-

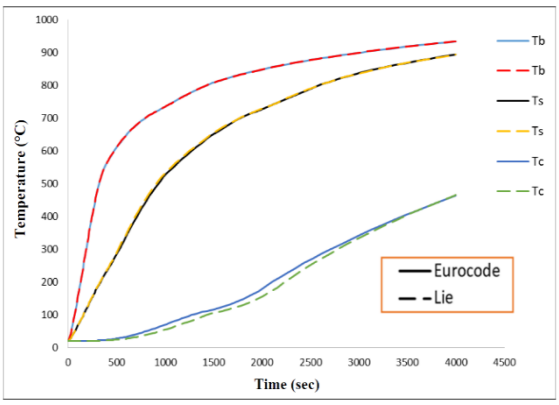

(e) Frame3

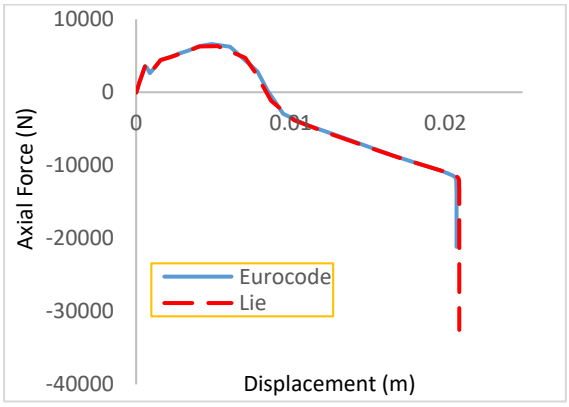

(f) Frame3

Fig. 12 Comparison of results of temperature-time between Eurocode and Lie: (a), (c), (e), and comparison of results of axial force-displacement between Eurocode and Lie: (b), (d), (f).

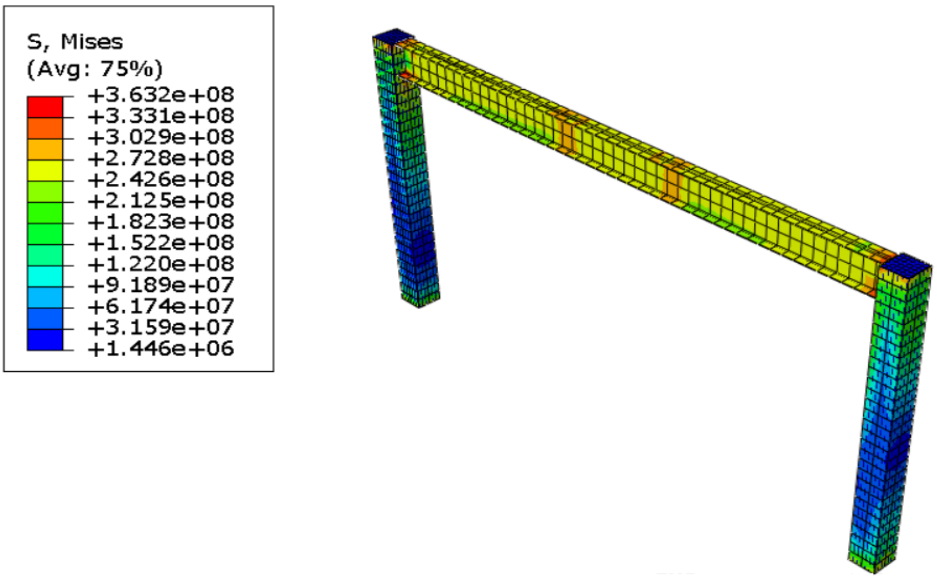

Fig. 13 Frame image in frame1 numerical model at 126 seconds

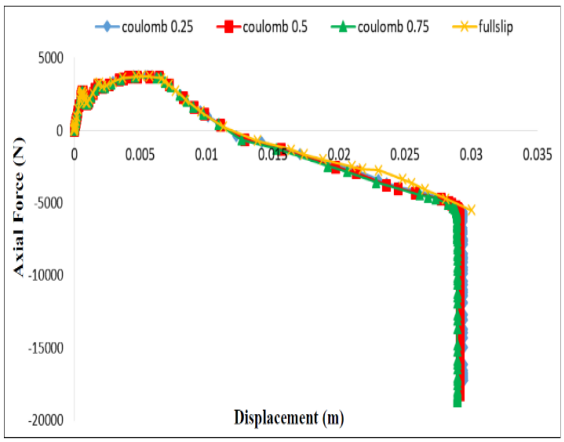

(a)

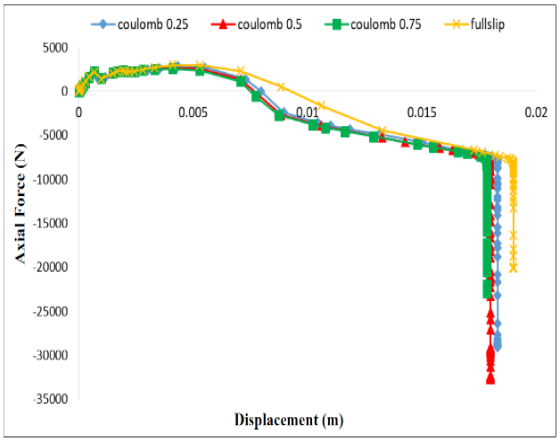

(b)

Continued-

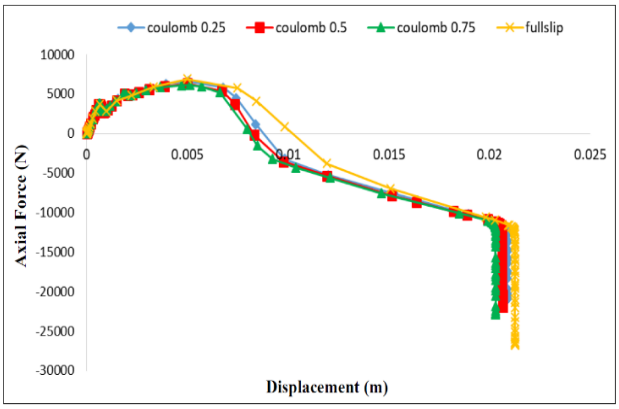

(c)

Fig. 14 Effects of friction coefficient in frames: (a) frame1, (b) frame2 and (c) frame3

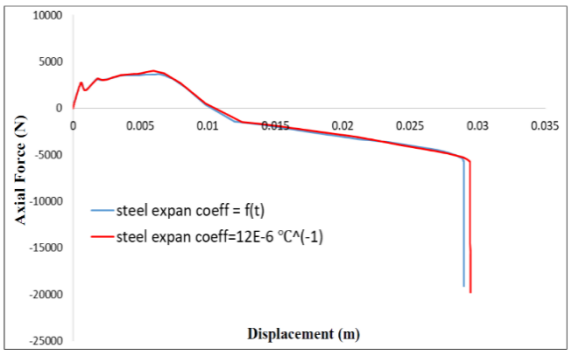

(a)

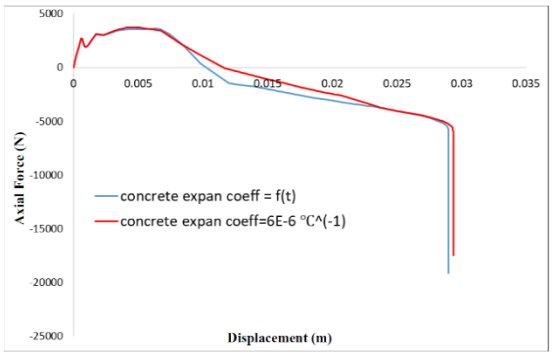

(b)

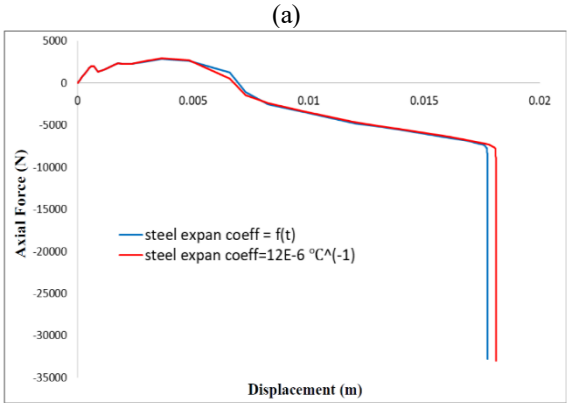

(c)

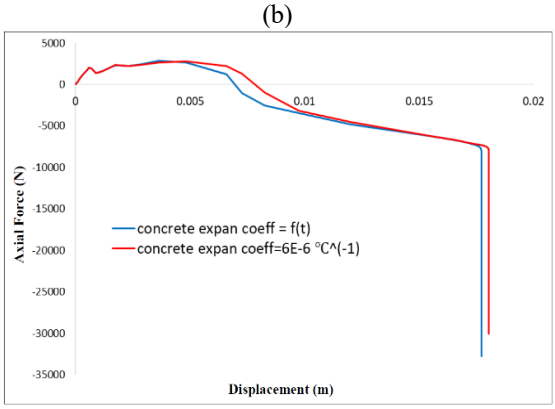

(d)

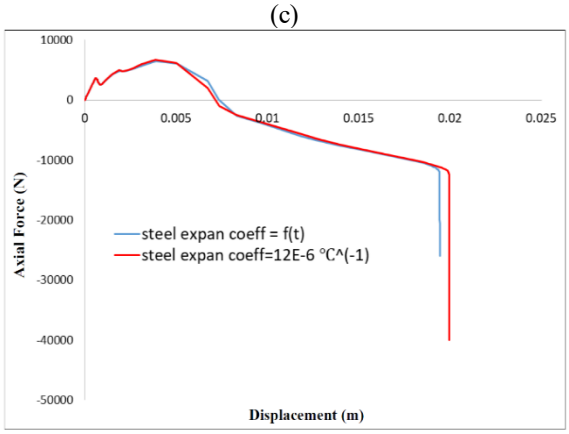

(e)

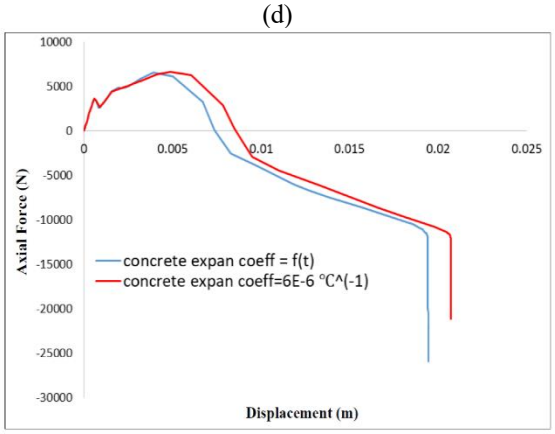

(f)

Fig. 15 Results of models compared to different steel thermal expansion coefficients: (a) Frame 1, (c) Frame2, (e) Frame3, and results of models compared to different concrete thermal expansion coefficients: (b) Frame1, (d) Frame2, (f) Frame3

Table 5 Failure time of models in studied parameters

Parameters investigated	Frame	Model	Fire resistance rating(sec)
Compressive strength of concrete	1	M1	3916
		M2	3721
	2	M1	2408
		M2	2253
	3	M1	2764
		M2	2486
Moisture content of concrete	1	M1	3916
		M2	*
	2	M1	2408
		M2	2623
	3	M1	2764
		M2	2940
Thermal conductivity	1	Eurocode	3916
		Lie	3911
	2	Eurocode	2408
		Lie	2421
	3	Eurocode	2764
		Lie	2788
Friction coefficient	1	Coulomb 0.25	3923
		Coulomb 0.5	3884
		Coulomb 0.75	3858
		fullslip	*
	2	Coulomb 0.25	2441
		Coulomb 0.5	2398
		Coulomb 0.75	2378
		fullslip	2533
	3	Coulomb 0.25	2783
		Coulomb 0.5	2752
		Coulomb 0.75	2707
		fullslip	2835
Thermal expansion coefficient**	1	f(t)	3866
		S	3927
		C	3916
	2	f(t)	2364
		S	2413
		C	2408
	3	f(t)	2592
		S	2662
		C	2764
Thermal gap	1	100	*
		200	3916
		500	3715
	2	100	2601
		200	2408
		500	2315
	3	100	3019
		200	2764
		500	2623

*: The model did not fail in 4000 seconds.
**: Different thermal expansion coefficients; f (t): Variable with temperature, (s): Constant coefficient of steel, (c): Constant coefficient of concrete

4. Conclusions

The obtained results in details are as follows:

-In the frames, first, the steel of column is enlarged due to the higher thermal expansion coefficient than concrete. Then, it resists to the point where the strength is decreased, which reduces the length of column steel. From this point onwards, the concrete goes into action and shows more resistance to the extent that the frame reaches the failure or rupture due to the applied axial load and the formed hinge in the beam near the point of the beam-column connection.

-In the frames, the 3 and 10% moisture content of concrete was studied. In models, the higher moisture content of the concrete reduces both the concrete temperature and the steel column temperature relative to the lower moisture content, and this decrease in temperature

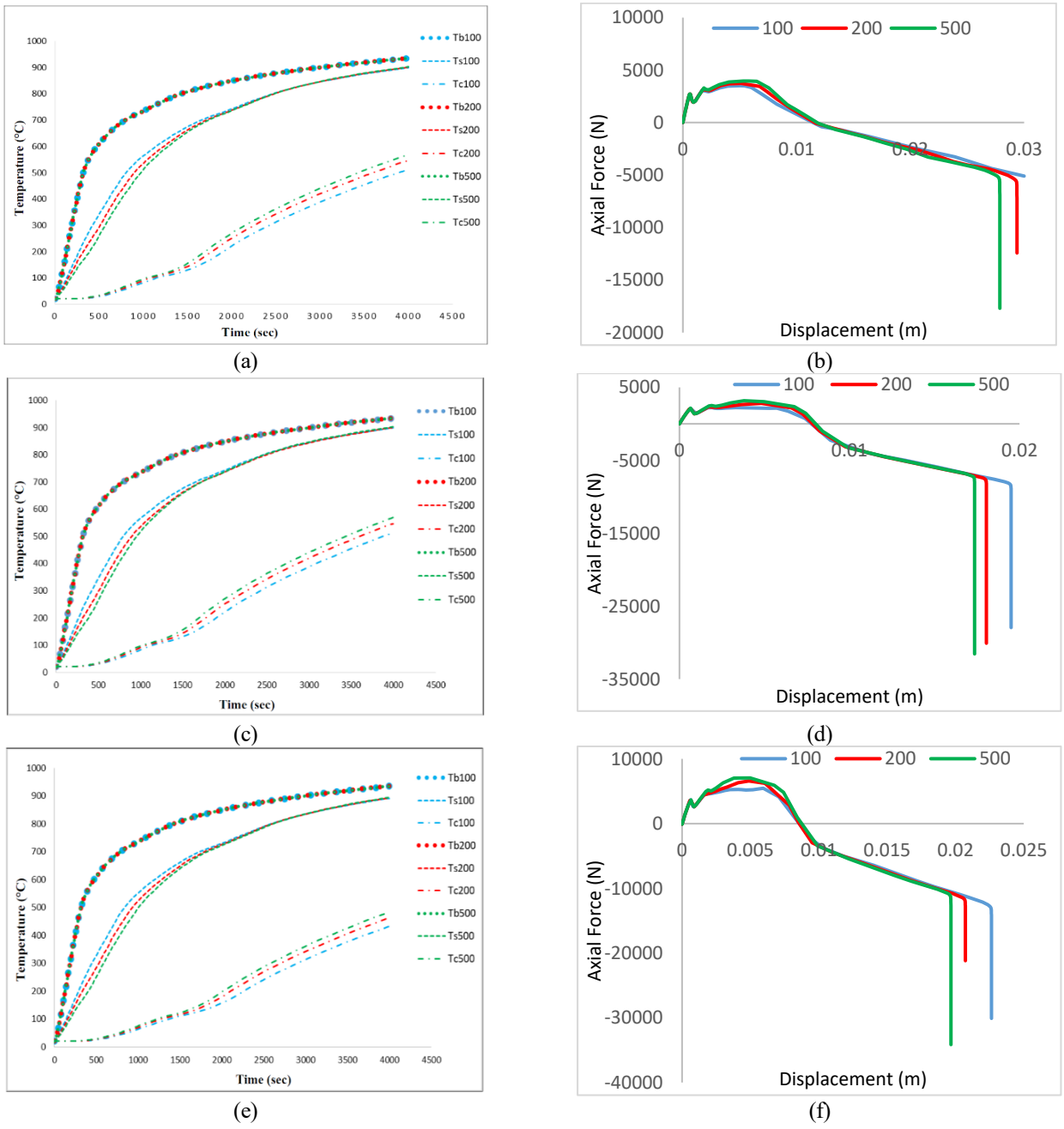

Fig. 16 Comparison of temperature-time results between points determined with different thermal gaps: (a), (c), (e), and comparison of results of axial force-displacement for models with different thermal gaps: (b), (d), (f)

causes the frame to show better performance against fire and fail later. In the first frame, the model m2 performs better than the model m1, so that the model did not fail after 4000 seconds under heating condition. In the second frame, model M2 with 10% moisture had a better performance with respect to model m1 with 3% moisture, and the structure failure time occurred with 8% delay. In the third frame also the failure time of model m2 with 10% moisture had a delay of 6% with respect to model m1 with 3% moisture.

-The thermal conductivity of Lie and Eurocode was analyzed for the models. It was found that there is no significant difference between the results of Lie and Eurocode. However, the greater the applied load, the sooner the results obtained from the Eurocode, though very little, are yielded than those of Lie.

-Two cases of friction, including Coulomb friction and the slip, were investigated for the frames. The results of Coulomb friction coefficients indicate that there is no significant difference in the response of the models. The results of the full slip for the models reveal that non-consideration of the friction between concrete and steel shows different results in comparison with the Coulomb friction. In the first frame, the full-slip model exhibited better performance than the considered values for the friction. Regarding the second frame, the failure time of the

full-slip model increased by 3, 5, and 6% more than those of the 0.25, 0.5, and 0.75 models, respectively. In terms of the third frame, the corresponding values were 2, 3, and 4.5%, respectively.

-The coefficient of thermal expansion of steel and concrete was analyzed. Two types of thermal expansion coefficients were considered for the models, in which the first one is constant, and the second is variable with temperature. The variable-temperature thermal expansion coefficient in comparison with the constant thermal expansion coefficient of concrete shows more variations than the constant thermal expansion coefficient of the steel. Besides, the constant thermal expansion coefficients for steel and concrete improve the failure time of the models to a minimal extent compared to the variable-temperature thermal expansion coefficient.

-The results of the thermal gap models indicate that with increasing the amount of thermal gap, the models will sooner lose their strength and fail.

References

Abdollahzadeh, G. and Afaghi-Darabi, A. (2018a), "Effect of drywall and brick wall on fire behavior of concrete-filled steel tube column", *Struct.Concrete*, **19**(3), 851-863.

Abdollahzadeh, G., Yapang-Gharavi, S. and Hoseinali-Beygi, M. (2018b), "Combination of mechanical and informational modeling to predict hysteresis behavior of I beam-to-CFT column connection", *Struct. Des. Tall Spec. Build*., **27**(3), e1420.

Arabnejad Khanouki, M.M., Ramli Sulong, N.H. and Shariati, M. (2010), "Investigation of seismic behaviour of composite structures with concrete filled square steel tubular (CFSST) column by push-over and time-history analyses", *Proceedings of the 4th International Conference on Steel & Composite Structures*.

Arabnejad Khanouki, M.M., Ramli Sulong, N.H. and Shariati, M. (2011), "Behavior of through Beam Connections Composed of CFSST Columns and steel beams by finite element studying", *Adv. Mater. Res*., **168**, 2329-2333 http://dx.doi.org/10.4028/www.scientific.net/AMR.168-170.2329.

ASTM, A. (2001), "Standard methods of fire test of building construction and materials".

Davoodnabi, S.M., Mirhosseini, S.M. and Shariati, M. (2019), "Behavior of steel-concrete composite beam using angle shear connectors at fire condition", *Steel Compos. Struct*., **30**(2), 141-147 https://doi.org/10.12989/scs.2019.30.2.141.

Ding, J. and Wang, Y. (2008), "Realistic modelling of thermal and structural behaviour of unprotected concrete filled tubular columns in fire", *J. Constr. Steel Res*., **64**(10), 1086-1102.

Elremaily, A. and Azizinamini, A. (2002), "Behavior and strength of circular concrete-filled tube columns", *J. Constr. Steel Res*., **58**(12), 1567-1591.

EN, B. (2004), "1-1. Eurocode 2: Design of concrete structures–Part 1-1: General rules and rules for buildings", European Committee for Standardization (CEN).

EN, C. (1994), "1-1, Eurocode 4: Design of composite steel and concrete structures", Part 1-1: General rules and rules for buildings2004.

En, C. (2005), "1-2, Eurocode 3: Design of steel structures, Part 1.2: General rules–Structural fire design", Brussels, Belgium: Comité Européen de Normalisation.

Espinos, A., Romero, M.L. and Hospitaler, A. (2010), "Advanced model for predicting the fire response of concrete filled tubular columns", *J. Constr. Steel Res*., **66**(8-9), 1030-1046.

Espinós, A., Romero, M.L., Portolés, J. and Hospitaler, A. (2014), "Ambient and fire behavior of eccentrically loaded elliptical slender concrete-filled tubular columns", *J. Constr. Steel Res*., **100**, 97-107.

Hajjar, J.F. (2000), "Concrete-filled steel tube columns under earthquake loads", *Progress in Structural Eng. Mater*., **2**(1), 72-81.

Han, L.H., Li, W. and Bjorhovde, R. (2014), "Developments and advanced applications of concrete-filled steel tubular (CFST) structures: Members", *J. Constr. Steel Res*., **100**, 211-228. https://doi.org/10.1016/j.jcsr.2014.04.016.

Han, L.H., Wang, W.D. and Zhao, X.L. (2008), "Behaviour of steel beam to concrete-filled SHS column frames: Finite element model and verifications", *Eng. Struct*., **30**(6), 1647-1658.

Han, L.H. and Yang, Y.F. (2005), "Cyclic performance of concrete-filled steel CHS columns under flexural loading", *J. Constr. Steel Res*., **61**(4), 423-452.

Han, L.H., Yao, G.H. and Tao, Z. (2007), "Performance of concrete-filled thin-walled steel tubes under pure torsion", *Thin-Wall. Struct*., **45**(1), 24-36.

Han, L.H., Zhao, X.L. and Tao, Z. (2001), "Tests and mechanics model for concrete-filled SHS stub columns, columns and beam-columns", *Steel Compos. Struct*., **1**(1), 51-74. https://doi.org/10.12989/scs.2001.1.1.051.

Hong, S. and Varma, A.H. (2009), "Analytical modeling of the standard fire behavior of loaded CFT columns", *J. Constr. Steel Res*., **65**(1), 54-69. https://doi.org/10.12989/scs.2009.65.1.054.

Ismail, M., Shariati, M., Abdul Awal, A.S.M., Chiong, C.E., Sadeghipour Chahnasir, E., Porbar, A., Heydari, A. and khorami, M. (2018), "Strengthening of bolted shear joints in industrialized ferrocement construction", *Steel Compos. Struct*., **28**(6), 681-690. https://doi.org/10.12989/scs.2018.28.6.681.

Katebi, J., Shoaei-parchin, M., Shariati, M., Trung, N.T. and Khorami, M. (2019), "Developed comparative analysis of metaheuristic optimization algorithms for optimal active control of structures", *Eng. with Comput*., 1-20.

Khorramian, K., Maleki, S., Shariati, M., Jalali, A. and Tahir, M. (2017), "Numerical analysis of tilted angle shear connectors in steel-concrete composite systems", *Steel Compos. Struct*., **23**(1), 67-85. https://doi.org/10.12989/scs.2017.23.1.067.

Kodur, V.K.R. and Lie, T.T. (1995), "Experimental studies on the fire resistance of circular hollow steel columns filled with steel-fibre-reinforced concrete", National Research Council Canada, Institute for Research in Construction.

Lai, M. and Ho, J. (2014), "Behaviour of uni-axially loaded concrete-filled-steel-tube columns confined by external rings", *Struct. Des. Tall Spec. Build*., **23**(6), 403-426.

Lam, D. and Williams, C.A. (2004), "Experimental study on concrete filled square hollow sections", *Steel Compos. Struct*., **4**(2), 95-112. https://doi.org/10.12989/scs.2004.4.2.095.

Lie, T. (1994), "Fire resistance of circular steel columns filled with bar-reinforced concrete", *J. Struct. Eng*., **120**(5), 1489-1509.

Lie, T. and Denham, E. (1993), "Factors affecting the fire resistance of circular hollow steel columns filled with bar-reinforced concrete".

Lie, T. and Stringer, D. (1994), "Calculation of the fire resistance of steel hollow structural section columns filled with plain concrete", *Can. J. Civil Eng*., **21**(3), 382-385.

Lie, T.T. and Chabot, M. (1990a), "Concrete filling: fire protection of hollow steel columns", *Can. Consulting Engineer*, 39-40.

Lie, T.T. and Chabot, M. (1990b), "A method to predict the fire resistance of circular concrete filled hollow steel columns", *J. Fire Protection Eng*., **2**(4), 111-124.

Lie, T.T. and Irwin, R. (1990c), "Evaluation of the fire resistance of reinforced concrete columns with rectangular cross-sections",

Luo, Z., Sinaei, H., Ibrahim, Z., Shariati, M., Jumaat, Z., Wakil, K.,

Pham, B.T., Mohamad, E.T. and Khorami, M. (2019), "Computational and experimental analysis of beam to column joints reinforced with CFRP plates", *Steel Compos. Struct*., **30**(3), 271-280. http://dx.doi.org/10.12989/scs.2019.30.3.271.

Mansouri, I., Shariati, M., Safa, M., Ibrahim, Z., Tahir, M. and Petković, D. (2019), "Analysis of influential factors for predicting the shear strength of a V-shaped angle shear connector in composite beams using an adaptive neuro-fuzzy technique", *J. Intel. Manufact*., **30**(3), 1247-1257.

Milovancevic, M., Marinović, J.S., Nikolić, J., Kitić, A., Shariati, M., Trung, N.T., Wakil, K. and Khorami, M. (2019), "UML diagrams for dynamical monitoring of rail vehicles", *Physica A: Stati. Mech. Appl*., 121169.

Naghipour, M., Yousofizinsaz, G. and Shariati, M. (2020), "Experimental study on axial compressive behavior of welded built-up CFT stub columns made by cold-formed sections with different welding lines", *Steel Compos. Struct*., **34**(3), 347-359. http://dx.doi.org/10.12989/scs.2020.34.3.347.

Qiao, Q., Li, X., Cao, W. and Dong, H. (2018), "Seismic behavior of specially shaped concrete-filled steel tube columns with multiple cavities", *Struct. Des. Tall Spec. Build*., **27**(12), e1485.

Romero, M.L., Espinós, A., Portolés, J., Hospitaler, A. and Ibañez, C. (2015), "Slender double-tube ultra-high strength concrete-filled tubular columns under ambient temperature and fire", *Eng. Struct*., **99**, 536-545.

Sajedi, F. and Shariati, M. (2019), "Behavior study of NC and HSC RCCs confined by GRP casing and CFRP wrapping", *Steel Compos. Struct*., **30**(5), 417-432. https://doi.org/10.12989/scs.2019.30.5.417.

Shahabi, S., Ramli Sulong, N.H., Shariati, M., Mohammadhassani, M. and Shah, S. (2016), "Numerical analysis of channel connectors under fire and a comparison of performance with different types of shear connectors subjected to fire", *Steel Compos. Struct*., **20**(3), 651-669. https://doi.org/10.12989/scs.2016.20.3.651.

Shariat, M., Shariati, M., Madadi, A. and Wakil, K. (2018), "Computational Lagrangian Multiplier Method by using for optimization and sensitivity analysis of rectangular reinforced concrete beams", *Steel Compos. Struct*., **29**(2), 243-256. https://doi.org/10.12989/scs.2018.29.2.243.

Shariati, M., Mafipour, M.S., Haido, J.H., Yousif, S.T., Toghroli, A., Trung, N.T. and Shariati, A. (2020), "Identification of the most influencing parameters on the properties of corroded concrete beams using an Adaptive Neuro-Fuzzy Inference System (ANFIS)", *Steel Compos. Struct*., **34**(1), 155-170. https://doi.org/10.12989/scs.2020.34.1.155.

Shariati, M., Mafipour, M.S., Mehrabi, P., Bahadori, A., Zandi, Y., Salih, M.N., Nguyen, H., Dou, J., Song, X. and Poi-Ngian, S. (2019a), "Application of a hybrid artificial neural network-particle swarm optimization (ANN-PSO) model in behavior prediction of channel shear connectors embedded in normal and high-strength concrete", *Appl. Sci*., **9**(24), 5534.

Shariati, M., Mafipour, M.S., Mehrabi, P., Shariati, A., Toghroli, A., Trung, N.T. and Salih, M.N. (2020), "A novel approach to predict shear strength of tilted angle connectors using artificial intelligence techniques", *Eng. Comput*., 1-21. https://doi.org/10.1007/s00366-019-00930-x.

Shariati, M., Mafipour, M.S., Mehrabi, P., Zandi, Y., Dehghani, D., bahadori, A., Shariati, A., Trung, N.T., Salih, M.N. and Poi-Ngian, S. (2019b), "Application of extreme learning machine (ELM) and Genetic Programming (GP) to design steel-concrete composite floor systems at elevated temperatures", *Steel Compos. Struct*., **33**(3), 319-332. https://doi.org/10.12989/scs.2019.33.3.319.

Shariati, M., Rafiei, S., Zandi, Y., Fooladvand, R., Gharehaghaj, B., Shariat, A., Trung, N.T., Salih, M.N., Mehrabi, P. and Poi-Ngian, S. (2019c), "Experimental investigation on the effect of cementitious materials on fresh and mechanical properties of self-consolidating concrete", Adv. concrete construction **8**(3), 225-237.

Shariati, M., Trung, N.-T., Wakil, K., Mehrabi, P., Safa, M. and Khorami, M. (2019d), "Moment-rotation estimation of steel rack connection using extreme learning machine", *Steel Compos. Struct*., **31**(5), 427-435. https://doi.org/10.12989/scs.2019.31.5.427.

Sinaei, H., Jumaat, M.Z. and Shariati, M. (2011), "Numerical investigation on exterior reinforced concrete Beam-Column joint strengthened by composite fiber reinforced polymer (CFRP)", *Int. J. Phys. Sci*., **6**(28), 6572-6579.

Standardization, E.C.f. (2004), "Design of concrete structures—Part 1-2: General rules—Structural fire design", EN 1992 Eurocode 2.

Talebi, E., Korzen, M. and Hothan, S. (2018), "The performance of concrete filled steel tube columns under post-earthquake fires", *J. Constr. Steel Res*., **150**, 115-128.

Tao, Z., Wang, Z.B. and Yu, Q. (2013), "Finite element modelling of concrete-filled steel stub columns under axial compression", *J. Constr. Steel Res*., **89**, 121-131.

Trung, N.T., Shahgoli, A.F., Zandi, Y., Shariati, M., Wakil, K., Safa, M. and Khorami, M. (2019), "Moment-rotation prediction of precast beam-to-column connections using extreme learning machine", *Struct. Eng. Mech*., **70**(5), 639-647. https://doi.org/10.12989/sem.2019.70.5.639.

Twilt, L., Hass, R., Klingsch, W., Edwards, M. and Dutta, D. (1994), "Design guide for structural hollow section columns exposed to fire. CIDECT Design Guide No. 4", Köln: TÜV-Verlag.

Wang, F.C. and Han, L.H. (2018), "Analytical behavior of special-shaped CFST stub columns under axial compression", *Thin-Wall. Struct*., **129**, 404-417.

Xie, Q., Sinaei, H., Shariati, M., Khorami, M., Mohamad, E.T. and Bui, D.T. (2019), "An experimental study on the effect of CFRP on behavior of reinforce concrete beam column connections", *Steel Compos. Struct*., **30**(5), 433-441. https://doi.org/10.12989/scs.2019.30.5.433.

Xu, C., Zhang, X., Haido, J.H., Mehrabi, P., Shariati, A., Mohamad, E.T., Nguyen, H. and Wakil, K. (2019), "Using genetic algorithms method for the paramount design of reinforced concrete structures", *Struct. Eng. Mech*., **71**(5), 503-513. https://doi.org/10.12989/sem.2019.71.5.503.

Ziaei-Nia, A., Shariati, M. and Salehabadi, E. (2018). "Dynamic mix design optimization of high-performance concrete", *Steel Compos. Struct*., **29**(1), 67-75. https://doi.org/10.12989/scs.2018.29.1.067.

CC